





Article

Comparing Transient and Steady-State Analysis of Single-Ring Infiltrometer Data for an Abandoned Field Affected by Fire in Eastern Spain

Simone Di Prima ^{1,*} , Laurent Lassabatere ², Jesús Rodrigo-Comino ³, Roberto Marrosu ¹, Manuel Pulido ⁴ , Rafael Angulo-Jaramillo ², Xavier Úbeda ⁵, Saskia Keesstra ^{6,7}, Artemi Cerdà ⁸  and Mario Pirastru ¹ 

¹ Dipartimento di Agraria, Università degli Studi di Sassari, Viale Italia 39, 07100 Sassari, Italy; rmarrosu@uniss.it (R.M.); mpirastru@uniss.it (M.P.)

² Université de Lyon, UMR5023 Ecologie des Hydrosystèmes Naturels et Anthropisés, CNRS, ENTPE, Université Lyon 1, 3 rue Maurice Audin, 69518 Vaulx-en-Velin, France; laurent.lassabatere@entpe.fr (L.L.); rafael.angulojaramillo@entpe.fr (R.A.-J.)

³ Department of Geography, Instituto de Geomorfología y Suelos, Málaga University, Campus of Teatinos, 29071 Málaga, Spain; rodrigo-comino@uma.es

⁴ GeoEnvironmental Research Group, Faculty of Philosophy and Letters, University of Extremadura, Avda. de la Universidad, 10071 Cáceres, Spain; mapulidof@unex.es

⁵ Mediterranean Environmental Research Group (GRAM), Department of Physical Geography and Regional Geographic Analysis, University of Barcelona, Montalegre 6, 08001 Barcelona, Spain; xubeda@ub.edu

⁶ Team Soil Water and Land Use, Wageningen Environmental Research, Wageningen UR, Droevendaalsesteeg 3, 6700 AA Wageningen, The Netherlands; saskia.keesstra@wur.nl

⁷ Civil, Surveying and Environmental Engineering, The University of Newcastle, Callaghan 2308, Australia

⁸ Soil Erosion and Degradation Research Group, Department of Geography, Valencia University, Blasco Ibáñez, 28, 46010 Valencia, Spain; artemio.cerda@uv.es

* Correspondence: sdiprima@uniss.it; Tel.: +39-079-229387

Received: 3 April 2018; Accepted: 18 April 2018; Published: 20 April 2018



Abstract: This study aimed at determining the field-saturated soil hydraulic conductivity, K_{fs} , of an unmanaged field affected by fire by means of single-ring infiltrometer runs and the use of transient and steady-state data analysis procedures. Sampling and measurements were carried out in 2012 and 2017 in a fire-affected field (burnt site) and in a neighboring non-affected site (control site). The predictive potential of different data analysis procedures (i.e., transient and steady-state) to yield proper K_{fs} estimates was investigated. In particular, the transient WU1 method and the BB, WU2 and OPD methods were compared. The cumulative linearization (CL) method was used to apply the WU1 method. Values of K_{fs} ranging from 0.87 to 4.21 mm·h⁻¹ were obtained, depending on the considered data analysis method. The WU1 method did not yield significantly different K_{fs} estimates between the sampled sites throughout the five-year period, due to the generally poor performance of the CL method, which spoiled the soil hydraulic characterization. In particular, good fits were only obtained in 23% of the cases. The BB, WU2 and the OPD methods, with a characterization based exclusively on a stabilized infiltration process, yielded an appreciably lower variability of the K_{fs} data as compared with the WU1 method. It was concluded that steady-state methods were more appropriate for detecting slight changes of K_{fs} in post-fire soil hydraulic characterizations. Our results showed a certain degree of soil degradation at the burnt site with an immediate reduction of the soil organic matter and a progressive increase of the soil bulk density during the five years following the fire. This general impoverishment resulted in a slight but significant decrease in the field-saturated soil hydraulic conductivity.

Keywords: post-fire soil hydraulic characterization; infiltration; bottomless bucket method; single-ring infiltrometer; field-saturated soil hydraulic conductivity; data analysis procedures

1. Introduction

Assessing the effects of fire on soil hydraulic properties in the Mediterranean area is crucial to evaluate the role of fire in land degradation and erosion processes. Among the soil hydraulic properties, field-saturated hydraulic conductivity, K_{fs} , exerts a key role in the partitioning of rainfall into runoff and infiltration [1]. Therefore, estimates of K_{fs} are essential for evaluating the hydrological response of fire-affected soils [2]. Soil properties are highly affected by fires due to the removal of the aboveground vegetation, the heat impact on the soil, the removal of the organic matter, the ash cover and the changes induced by rainfall on the soil surface [3–5]. Most of the research carried out on fire-affected land has paid attention to the “window of disturbance”, which is the period during which the soil losses are higher than before the fire and which lasts for a few years [6–8]. In order to understand the evolution of soil erosion after forest fires it is necessary to monitor fire-affected sites over a long period of time, in order to enable the assessment of the period affected by the window of disturbance [9]. Moreover, it is also possible to carry out measurements and experiments in areas with a different fire history. This gives information about the temporal changes in soil erosion after fire.

For this purpose, speed and ease of field procedures for soil hydraulic characterization are essential [10,11]. The single-ring infiltrometer technique [12,13] is a routinely used method for measuring K_{fs} in the field (e.g., [14–17]). With a single-ring infiltrometer, a constant or falling-head infiltration process has to be established. In the field, a constant-head single-ring infiltrometer often needs level-control setups or expensive devices with monitoring equipment containing proprietary technology with prohibitive costs [18–20]. Therefore, a falling-head experiment is preferable since it minimizes the complexity of implementation, characterizing an area of interest with minimal experimental efforts [11,21]. Recently, Nimmo et al. [11] developed the so-called bottomless bucket, named BB method hereafter, which uses a portable, falling-head, small-diameter single-ring infiltrometer. These authors adapted the Reynolds and Elrick (1990) formula to be applied instantaneously during a falling-head test. However, only few comparisons of BB estimates with other procedures can be found in the literature (e.g., [2,22]), notwithstanding that this method of soil hydraulic characterization is of noticeable practical interest. In general, establishing the reliability of new methods is not a simple task, also due to the high K_{fs} variability both in space and time [23,24]. Moreover, many other sources of variability may also arise when comparing different field measurement techniques, such as sample size [25], ring diameter [26], source shape [27] and field sampling procedure [28,29]. One could expect that considering laboratory measurements as targeted values would help to check the reliability of field data. However, this approach may be questioned due to the difficulty of representing the soil heterogeneity encountered in the field in small-scale laboratory samples (e.g., [24,30–33]). An alternative approach, considering different calculation techniques applied to the same dataset, is expected to facilitate the interpretation arising from the comparison [24]. Different methods of calculating K_{fs} from single-ring data were developed over time (e.g., [10–12,21,34–37]). Among them, the one ponding depth (OPD) calculation approach of Reynolds and Elrick [12] and Method 2 by Wu et al. [38] (WU2) have in common with the BB method that all these approaches analyze steady-state single-ring infiltrometer data, thus considering the same part of the infiltration process [24]. Moreover, they all require an estimate of the sorptive number (or macroscopic capillary length parameter), α^* (L^{-1}), expressing the relative importance of gravity and capillary forces during a ponding infiltration process [1].

The general objective of this work was to determine the K_{fs} of an abandoned unmanaged field affected by fire by means of single-ring infiltrometer runs and the use of transient and steady-state data analysis procedures. Sampling and measurements were carried out in 2012 and 2017 in a fire-affected

(on 15 July) field (burnt site) and in a neighboring non-affected site (control site). The focus was put on the predictive potential of different data analysis procedures (i.e., transient and steady-state) to yield proper K_{fs} estimates and to detect the effect of fire on saturated hydraulic conductivity. More specifically, we chose to test the bottomless bucket method by comparing the field-saturated soil hydraulic conductivity estimates with those obtained by other well-tested methods.

2. Theory

2.1. Steady-State Analysis of Single-Ring Infiltrometer Data

The bottomless bucket method of Nimmo et al. [11] considers the analysis developed by Reynolds and Elrick [12] of three-dimensional (3D), steady, ponded infiltration below a finite insertion depth, accounting for the hydrostatic pressure of the ponded water, gravity and capillarity of the unsaturated soil [1]. These authors adapted Reynolds and Elrick's (1990) formula to be applied instantaneously during a falling-head test. With this method, K_{fs} ($L \cdot T^{-1}$) is calculated by the following equation:

$$K_{fs} = \frac{L_G}{t} \ln \left(\frac{L_G + \lambda_c + H_0}{L_G + \lambda_c + H} \right) \quad (1)$$

where H_0 (L) is the initially established ponded depth of water, $H(t)$ (L) is the ponded depth of water at time t , λ_c (L) is the macroscopic capillary length of the soil [39], and the so-called ring installation scaling length, L_G (L), is calculated as follow:

$$L_G = 0.316\pi d + 0.184\pi r \quad (2)$$

where r (L) is the radius of the disk source and d (L) is the ring insertion depth in the soil.

The one ponding depth calculation approach by Reynolds and Elrick [12] makes use of the steady infiltrating flux, Q_s ($L^3 \cdot T^{-1}$), which is estimated from the flow rate versus time plot. The following relationship is used to obtain K_{fs} :

$$K_{fs} = \frac{\alpha * \gamma_G Q_s}{r(\alpha * H + 1) + \gamma_G \alpha * \pi r^2} \quad (3)$$

where γ_G is a shape factor that can be estimated as follows:

$$\gamma_G = 0.316 \frac{d}{r} + 0.184 \quad (4)$$

Method 2 by Wu et al. [38] assumes steady-state infiltration. With this method, K_{fs} is calculated by the following equation:

$$K_{fs} = \frac{i_s}{af} \quad (5)$$

where i_s ($L \cdot T^{-1}$) is the slope of the straight line fitted to the data describing steady-state conditions on the cumulative infiltration, I (L), versus time, t (T), relation, a is a dimensionless constant equal to 0.9084 [36], and f is a correction factor that depends on soil initial and boundary conditions and ring geometry:

$$f \cong \frac{H + 1/\alpha *}{G^*} + 1 \quad (6)$$

where the G^* (L) term is equal to:

$$G^* = d + \frac{r}{2} \quad (7)$$

2.2. Transient Analysis of Single-Ring Infiltrometer Data

For comparative purposes, Method 1 by Wu et al. [38] (WU1) was also applied to estimate K_{fs} . In addition, this method offered the possibility to check the assumed α^* value by directly estimating this parameter from a single-ring test and a measurement of the soil water content. This method is based on the assumption that the cumulative infiltration can be described by a relation formally identical to the two-term infiltration model by Philip [40]:

$$I = C_1\sqrt{t} + C_2t \quad (8)$$

where C_1 ($L \cdot T^{-0.5}$) and C_2 ($L \cdot T^{-1}$) are infiltration coefficients. With method 1, K_{fs} is calculated by the following equation:

$$K_{fs} = \frac{\lambda_c \Delta\theta}{T_c} \quad (9)$$

where $\Delta\theta$ ($L^3 \cdot L^{-3}$) is the difference between the saturated volumetric soil water content, θ_s ($L^3 \cdot L^{-3}$), and the initial one, θ_i ($L^3 \cdot L^{-3}$). The λ_c (L) and T_c (T) terms have the following expressions:

$$\lambda_c = \frac{1}{2} \left[\sqrt{(H + G^*)^2 + 4G^*C} - (H + G^*) \right] \quad (10)$$

$$T_c = \frac{1}{4} \left(\frac{C_2 a}{b C_1} \right)^2 \quad (11)$$

where H (L) is the established ponding depth of water, G^* (L) is defined by Equation (7), a and b are dimensionless constants respectively equal to 0.9084 and 0.1682 [36], and the C (L) term is equal to:

$$C = \frac{1}{4\Delta\theta} \left(\frac{C_2}{b} \right)^2 \frac{a}{C_1} \quad (12)$$

An estimate of the sorptive number, α^* (L^{-1}), may also be obtained taking into account that:

$$\alpha^* = \frac{1}{\lambda_c} \quad (13)$$

For a given infiltration run we determined the C_1 and C_2 coefficients according to the fitting method referred to as cumulative linearization (CL, [41]). With the CL method, Equation (8) is linearized by dividing both sides by \sqrt{t} , giving:

$$\frac{I}{\sqrt{t}} = C_1 + C_2\sqrt{t} \quad (14)$$

Then, the C_1 and C_2 coefficients are determined respectively as the intercept and the slope of the I/\sqrt{t} vs. \sqrt{t} plot.

3. Materials and Methods

3.1. Soil Sampling

We selected two study sites on abandoned fields within the “Serra de Mariola Natural Park” in Alcoi, Eastern Spain. The coordinates of the study area are $38^\circ 43' 32.15''$ N, $0^\circ 28' 54.70''$ W. Sampling and measurements were carried out in November 2012 and five years later, in November 2017, in a fire-affected (on 15 July) field (burnt site) and in a neighboring non-affected site (control site). The study area is characterised by typical Mediterranean climatic condition with drought from June till September, with high temperatures (25°C in average), and mild spring, autumn and winter seasons. The mean annual rainfall at the nearby Cocentaina meteorological station is 480 mm, and during the

study period the mean annual rainfall was 418 mm. The wettest year was 2012 with 576 mm and the driest 2014 with 209 mm. October used to be the month with the largest rainfall amount, although during the study period the wettest month was December 2015 with 295 mm, and the driest months were May 2017 and July 2014 with 0 mm of rainfall. Mean monthly rainfall data are reported in Figure 1. The mean monthly temperature was 16.5 °C, with values in July of 28.3 °C and January with 7.0 °C. The vegetation cover was dominated by a scrubland developed after the abandonment that took place in 1950s. The main plant species were *Rosmarinus officinalis*, *Thymus vulgaris*, and *Ulex parviflorus*, and five years after the fire the vegetation was dominated by *Cistus albidus*, although *Rosmarinus officinalis* and *Ulex parviflorus* were also present.

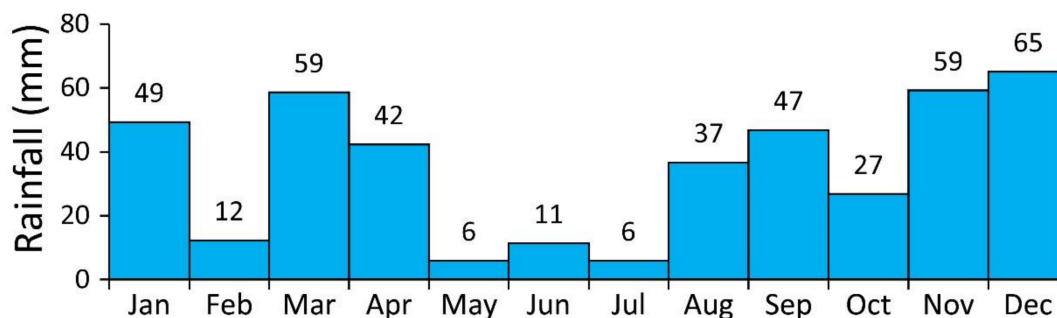


Figure 1. Mean monthly rainfall data recorded at the Cocentaina meteorological station during the study period (2012–2017).

The parent material is marls and the soils developed on this south-facing slope are very breakable. The soil is classified as a Typic Xerorthent [42]. According to the USDA standards, the three fractions, i.e., clay (0–2 µm), silt (2–50 µm) and sand (50–2000 µm), averaged for the two sites were 14.5%, 57.5% and 29.1%, respectively (corresponding standard deviations = 6.6, 4.3 and 5.0, respectively), and the soil of the studied area was classified as silt loam.

Plant cover was measured at each sampling point prior to infiltration experiments by measuring the presence (1) or absence (0) at 100 points regularly distributed in each 0.28 m² plot. Undisturbed soil cores were also collected at 0–60 mm soil depth. The cores were used to determine the soil bulk density, ρ_b (g·cm⁻³), and the initial volumetric soil water content, θ_i (m³·m⁻³). According to other investigations, the saturated soil water content, θ_s (m³·m⁻³), was approximated by total soil porosity, determined from bulk density ρ_b (e.g., [28,37,43–48]). Soil organic matter was determined by the Walkley-Black [49] method.

3.2. Single-Ring Infiltrometer

A total of forty infiltration runs (10 runs × 2 plots × 2 sampling campaigns) of the bottomless bucket type were carried out [11]. A 100-mm inner diameter ring was inserted into the soil to a depth of $d = 50$ mm. At the start of the experiments, water was poured into the ring to establish an initial ponding depth $H_0 = 50$ mm. In this investigation, the possible occurrence of soil water repellency was not considered, given that this phenomenon is uncommon for scrub terrain on calcareous soils in the region, even after fire [50,51]. Therefore, the use of ponding experiments, which are known to overwhelm positive soil-water-entry values induced by water repellency (e.g., [2,52–54]), was not expected to induce bias. The rate of drop of the water level was monitored by measuring the ponding depth at prescribed time intervals, $H(t)$. After each measurement, another volume of water was poured immediately into the ring to re-establish a ponded depth of water of 50 mm. During the first minutes, small time intervals were used. The time interval was increased up to 5 min in the late phase of the experiment. Steady-state conditions were attained within 60 min of all experiments. This procedure differs from the one proposed by Nimmo et al. [11], since these authors logged the time needed for

the water to reach a minimum fixed $H(t)$ value, thus pouring in known water volumes to re-establish the initial ponding depth. The obvious advantage to consider prescribed time intervals instead of a preselected water amount, is that monitoring time is significantly easier than monitoring water levels. Moreover, in their investigation Nimmo et al. [11] stated that the “modification of these procedures is likely to be necessary for different soils and conditions”. In our case, the sampled soils were characterized by low permeability. In such conditions, logging the time needed for the water to reach a minimum fixed $H(t)$ value, such as the Nimmo’s procedure, would imply obtaining less data points for the same duration of the experiment, or alternatively it would imply considerably extending the experiment duration to have a similar number of data points and, thus, to properly evaluate the steady-state phase of the infiltration process. Therefore, the applied criterion also allowed us to increase our confidence in the sampled data. A total of forty experimental cumulative infiltrations versus time were then deduced. Cumulative infiltration data were firstly analyzed according to the criterion suggested by Bagarello et al. [55]. Specifically, apparent steady-state infiltration rates were estimated by linear regression analysis of the last three (I, t) data points. Then, the equilibration time, t_s (min), namely the duration of the transient phase of the infiltration process, was determined as the first value for which:

$$\left| \frac{I - I_{reg}}{I} \right| \times 100 \leq E \tag{15}$$

where I_{reg} is estimated from the regression analysis of the I versus t plot, and E is a criterion to check linearity. Equation (15) is applied from the start of the experiment and progressively excludes the first data points until $E \leq 2$ [1,24]. An illustrative example of the t_s estimation is reported in Figure 2.

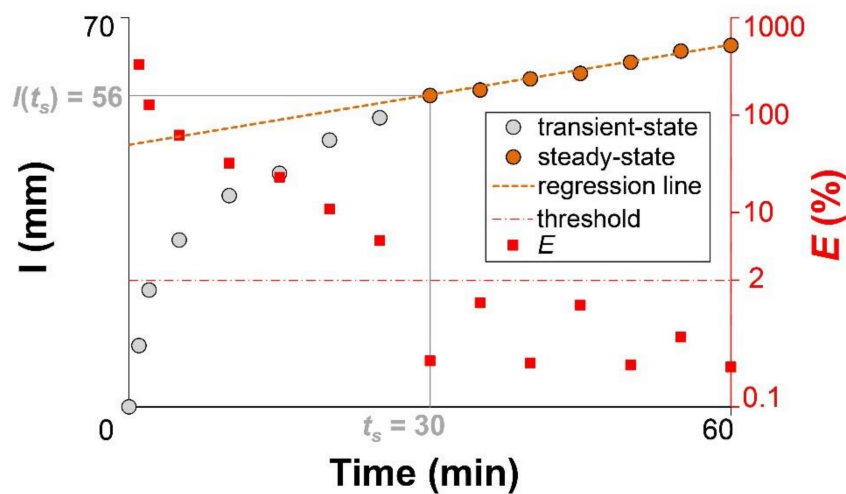


Figure 2. Procedure for estimating equilibration time, t_s (min), and infiltrated depth at the equilibration time, $I(t_s)$ (mm), from cumulative infiltrations. Case of an infiltration run carried out at the burnt site in 2012.

3.3. Data Analysis and Calculations

The BB procedure was applied to determine K_{fs} (K_{fs-BB}) by Equation (1), assuming $\lambda_c = 1/\alpha^* = 0.25$ m. A value of $\alpha^* = 4 \text{ m}^{-1}$ for unstructured fine-textured soils (strong soil capillarity category) was selected from the soil texture–structure categories defined by Elrick and Reynolds [56]. The last determinations of K_{fs-BB} , representative of steady-state conditions, were averaged to obtain an estimate of K_{fs-BB} for a given test, as suggested by Angulo-Jaramillo et al. [1].

Equations (3) and (5) were applied to estimate K_{fs} data, which were denoted with the symbols K_{fs-WU2} and K_{fs-OPD} , for WU2 and OPD, respectively. It has to be noted that these latter methods are theoretically usable for a constant ponded depth of water on the infiltration surface.

However, in our case, the variation of the water level during the late-phase of the infiltration process never exceeded 1–2 mm. Therefore, the ponded depth at the late-phase of the run was assumed to be practically constant.

For comparative purposes, the transient WU1 method was also applied to estimate K_{fs} and α^* by Equations (9) and (13), respectively. These estimates were denoted with the symbols $K_{fs-WU1-CL}$ and α^*_{CL} . We first obtained the C_1 and C_2 values with the CL method by fitting Equation (14). The adequacy of the fitting procedure was evaluated by checking both the linearity of the data and the relative error defined as:

$$Er = 100 \times \sqrt{\frac{\sum_{i=1}^n (x_i^{\text{exp}} - x_i)^2}{\sum_{i=1}^n (x_i^{\text{exp}})^2}} (i = 1..n) \quad (16)$$

where x_i^{exp} are the experimental data and x_i are the corresponding values deduced by fitting the functional relationship. According to the criterion proposed by Lassabaterre et al. [10], values of $Er < 5\%$ were assumed to be indicative of a satisfactory fitting ability.

The statistical frequency distributions of the K_{fs} and α^* data were assumed to be lognormal, as is common for these variables (e.g., [57,58]). Therefore, geometric means and associated coefficients of variation, CV, were calculated using the appropriate “log-normal equations” [59]. The other variables considered in this investigation were summarized by calculating the arithmetic mean and the associated CV, since the characterization of an area of interest is generally based on arithmetic averages of individual determinations [60]. To compare mean values, untransformed and natural log-transformed data were used for the normal and the natural log-normal distributed variables, respectively. Different K_{fs} datasets were also compared in terms of factors of difference (FoD), calculated as the ratio between the maximum and minimum of two K_{fs} values estimated by different calculation techniques from a run [24]. Following Elrick and Reynolds [56], FoD values not exceeding a factor of two or three were considered indicative of similar estimates.

4. Results

4.1. Physical Properties

The results of the physical analysis were represented using box plot graphics (Figure 3). A major effect of fire was a consistent reduction of soil organic matter in the burnt site. SOM was measured to decrease by 22% four months after the fire, and 30% after five years. This reduction was in line with previous investigations (e.g., [3,61–63]). As a consequence, dryer conditions persisted in the burnt site, due to the known effect of a reduction of soil organic matter on soil water retention [64]. Specifically, the initial soil water content differed appreciably among the control and burnt sites, with average θ_i values equal to 0.141 and 0.137 $\text{m}^3 \cdot \text{m}^{-3}$ at the control site and 0.096 and 0.087 $\text{m}^3 \cdot \text{m}^{-3}$ at the burnt site, for the 2012 and 2017 sampling campaigns, respectively. No significant differences in terms of soil dry bulk density were detected between the control and burnt sites four months after the fire. On the contrary, our results showed a significant increase of the bulk density five years after the fire, due probably to a progressive collapse of aggregates [9], highlighting a certain degree of soil degradation at the burnt site.

4.2. Performance of the Cumulative Linearization (CL) Method

The application of the transient WU1 method to determine K_{fs} and α^* required the estimation of the C_1 and C_2 coefficients. We obtained the C_1 and C_2 values with the CL fitting method. This method showed general poor performance both in terms of the linearity of the data and the relative error. The $\Delta I / \Delta \sqrt{t}$ vs. \sqrt{t} plots did not show the expected linear relationship between the considered variables for the entire infiltration run. Therefore, we progressively excluded the first data points selecting the C_1 and C_2 values when the following criteria were fulfilled: (i) positive values of the

C_2 parameter (yielding physically plausible K_{fs} estimates i.e., $K_{fs} > 0$); and (ii) a linear relationship between the considered variables. An example of the applied selection procedure for the infiltration coefficients is depicted in Figure 4. The example refers to the case of an infiltration run carried out at the burnt site in 2017. The exclusion of no or one data point yielded negative C_2 values (Figure 4a,b). The exclusion of two data points yielded a positive C_2 value, but a value of $Er = 6.6\%$ was obtained due to the departure of the first point from the general linear behaviour (Figure 4c). In this case, the C_2 coefficient should make it possible to obtain an apparently physically plausible K_{fs} estimate, i.e., $K_{fs} > 0$. However, given that the dataset was not linear, Equation (8) was considered inappropriate and hence the fitted parameters were considered as meaningless from a physical point of view [65]. Finally, the C_1 and C_2 coefficients could be properly estimated by excluding the first three data points (Figure 4d). Other investigations also suggested removing the fitting procedures the early stage of the infiltration process when a perturbation occurs (e.g., [21,38,46,66]). In contrast, the last points may be removed since the CL method mostly applies to the transient state [65,67]. Only one test never yielded positive C_2 values whatever the number of data points excluded. Good fits, i.e., fitting yielding Er values lower than 5% [10], were only obtained in 23% of the cases (Figure 5).

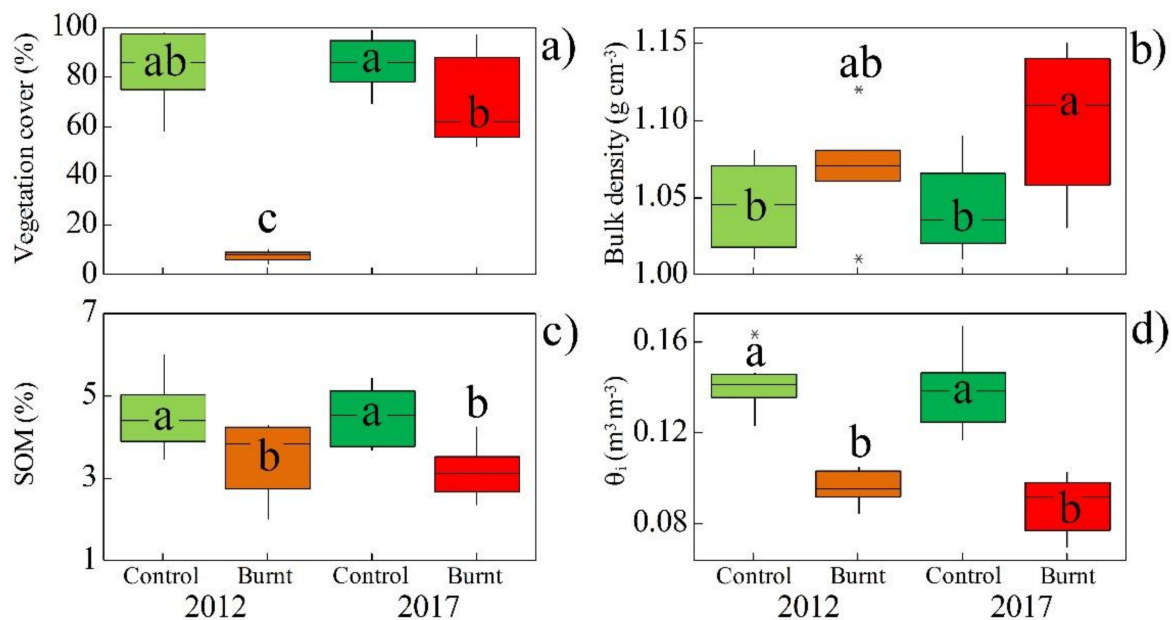


Figure 3. Box plots of the (a) vegetation cover (%), (b) soil bulk density ($g \cdot cm^{-3}$), (c) soil organic matter, (SOM) (%), and (d) initial volumetric soil water content, θ_i ($m^3 \cdot m^{-3}$), for the four scenarios. Asterisks denote outliers. Different letters represent significant differences at $p < 0.05$.

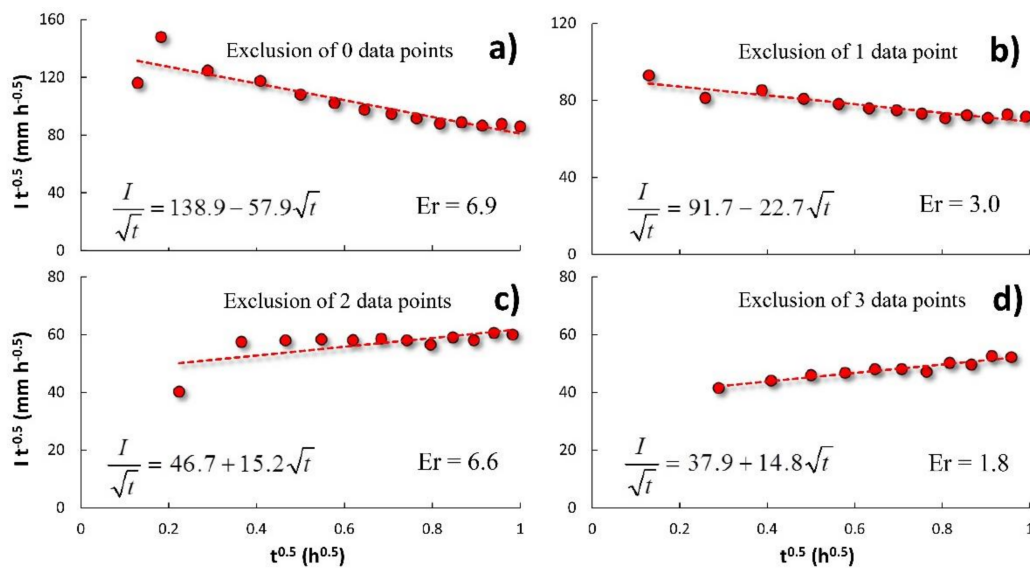


Figure 4. Examples of the estimation of the C_1 ($\text{mm}\cdot\text{h}^{-0.5}$) and C_2 ($\text{mm}\cdot\text{h}^{-1}$) parameters by the cumulative linearization (CL) approach excluding a different number of data points of an infiltration run carried out at the burnt site in 2017. The values of the ratio between the cumulative infiltration, I (mm), and the square root of time, t (h), are plotted against the square root of t . (a) Exclusion of zero data points: $C_2 < 0$. (b) Exclusion of one data point: Lower Er value (3.0%) but $C_2 < 0$. (c) Exclusion of two data points: $C_2 > 0$ but $Er = 6.6\%$. (d) Exclusion of three data points: $C_2 > 0$ and lowest Er value (1.8%; selected case).

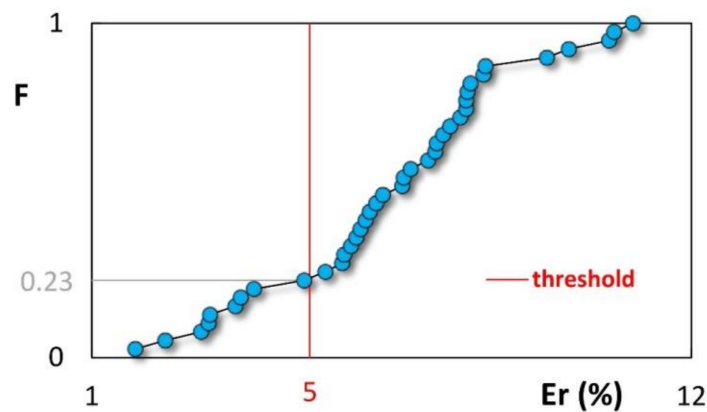


Figure 5. Cumulative frequency distribution of the relative errors, Er (%), of the fitting of the functional relationship (i.e., Equation (14)) for the CL method to the experimental data. Er values not exceeding 5% denote a satisfactory fitting ability of the infiltration model to the data [10].

4.3. Estimation of K_{fs} Data with the WU1 Method

Table 1 summarizes the field-saturated soil hydraulic conductivity obtained with the WU1 method. The average $K_{fs-WU1-CL}$ values ranged from 0.87 to 1.50 $\text{mm}\cdot\text{h}^{-1}$. All average K_{fs} values were lower than the expected saturated conductivity on the basis of the soil textural characteristics alone, e.g., $K_s = 4.5 \text{ mm}\cdot\text{h}^{-1}$ for a silt loam soil according to Carsel and Parrish [68]. This suggested that soil macroporosity in the control and burnt site did not influence the results [28]. All differences between the average K_{fs} values of different sites and sampling campaigns were not statistically significant according to the Tukey honestly significant difference test ($p < 0.05$). A high variability of K_{fs} was detected in most cases, with coefficient of variations (CVs) ranging from 100.7% to 373.1% (Table 1).

The average α^*_{CL} values ranged from 2.42 to 6.45 m^{-1} (Table 2). We never detected extremely unreliable α^* values, i.e., lower than 0.1 m^{-1} and higher than 1000 m^{-1} [56,69]. All differences between the average α^*_{CL} values of different sites and sampling campaigns were not statistically significant according to the Tukey honestly significant difference test ($p < 0.05$). Considering all the infiltration measurements, the average α^*_{CL} value was equal to 3.89 m^{-1} . This value was in line with the one suggested by Elrick and Reynolds [56] for strong capillarity soils ($\alpha^* = 4 m^{-1}$) in their soil texture–structure categories.

Table 1. Summary of the field-saturated hydraulic conductivity, K_{fs} ($mm \cdot h^{-1}$), values obtained by the WU1 method for each sampling campaign and site.

Variable	Year	Site	Statistic				
			N	min	max	mean	CV
$K_{sf-WU-CL}$	2012	Control	10	0.18	5.36	1.11	211.8
		Burnt	10	0.04	8.17	0.87	373.1
	2017	Control	10	0.17	2.85	0.91	100.7
		Burnt	9	0.28	7.73	1.50	158.0

All differences between two mean values were not statistically significant according to the Tukey honestly significant difference test ($p < 0.05$).

Table 2. Summary of the α^*_{CL} (m^{-1}) values obtained by the WU1 method for each sampling campaign and site.

Variable	Year	Site	Statistic				
			N	min	max	mean	CV
α^*_{CL}	2012	Control	10	0.90	79.99	6.45	436.8
		Burnt	10	0.74	21.29	2.94	131.7
	2017	Control	10	0.85	27.25	2.42	117.8
		Burnt	9	1.12	16.71	5.16	109.1

All differences between two mean values were not statistically significant according to the Tukey honestly significant difference test ($p < 0.05$).

4.4. Estimation of K_{fs} Data with Steady-State Methods

We discriminated the transient and steady-state phase of the infiltration process according to the criterion suggested by Bagarello et al. [55] (Figure 2). This procedure allowed us to consider, for a given run, exactly the same final part of the curve for all the three applied methods. After a duration of 60 min, the total infiltrated depth was, on average, 64 mm. The equilibration time, t_s (min), namely the duration of the transient phase of the infiltration process, was reached, on average, after 33 min, with a mean volume of infiltrated water $I(t_s) = 56$ mm. All the experiments exhibited a sufficiently long steady-state phase ranging from 10 to 45 min (Table 3).

Table 3. Summary of the equilibration time, t_s (min), and infiltrated depth at the equilibration time, $I(t_s)$ (mm). Sample size, $N = 10$ for each site and sampling campaign.

Variable	Year	Site	Statistic			
			min	max	mean	CV
t_s (min)	2012	Control	25	40	30.5	12.1
		Burnt	25	45	35.0	22.3
	2017	Control	20	50	33.5	29.9
		Burnt	15	45	32.5	32.6
$I(t_s)$ (mm)	2012	Control	29	86	61.9	22.0
		Burnt	36	59	49.8	17.2
	2017	Control	53	84	64.1	17.1
		Burnt	19	71	49.3	40.6

Table 4 summarizes the field-saturated soil hydraulic conductivity, K_{fs} , obtained with the BB, OPD and WU2 methods. The average K_{fs-BB} , K_{fs-OPD} and K_{fs-WU2} values ranged from 2.0 to 3.96, from 2.03 to 4.21 and from 1.92 to 3.91 $\text{mm}\cdot\text{h}^{-1}$, respectively. The applied methods yielded similar information, i.e., the differences between average K_{fs} values of the control site were never statistically significant at $p < 0.05$. On the contrary, for the burnt site, the field campaign carried out in 2017 yielded, in all cases, two times lower K_{fs} values than the previous campaign, and the differences between sampling campaigns were always statistically significant at $p < 0.05$ (Table 4). Figure 6 depicts the box plots of the factor of difference values, i.e., a “point-by-point” comparison between all K_{fs} datasets. FoD values never exceeded 1.3 between steady-state methods. Therefore, the three steady-state methods considered in this investigation yielded similar results, supporting the soundness of the BB analysis procedure. On the contrary, appreciably higher FoD values were obtained with the WU1 method (Figure 6). In this case, the high variability of the data affected K_{fs} comparisons between sites and sampling campaigns (Table 1).

Table 4. Summary of the field-saturated hydraulic conductivity, K_{fs} ($\text{mm}\cdot\text{h}^{-1}$), data sets obtained by the BB, WU2, and OPD methods. Sample size, $N = 10$ for each site and sampling campaign.

Variable	Year	Site	Statistic			
			min	max	mean	CV
K_{sf-BB}	2012	Control	1.52	4.99	3.04 AB	45.4
		Burnt	2.49	4.99	3.96 A	19.5
	2017	Control	2.18	5.35	3.62 A	31.6
		Burnt	0.83	8.01	2.00 B	68.7
K_{sf-WU2}	2012	Control	1.34	5.28	2.95 AB	59.5
		Burnt	2.64	5.16	4.21 A	20.6
	2017	Control	2.00	5.82	3.57 AB	39.1
		Burnt	0.88	8.91	2.03 B	74.7
K_{sf-OPD}	2012	Control	1.24	4.98	2.85 AB	56.2
		Burnt	2.49	4.98	3.91 A	19.9
	2017	Control	1.99	5.34	3.44 A	35.0
		Burnt	0.83	7.97	1.92 B	71.8

For a given method (BB, WU2 and OPD), means that do not share a letter are significantly different according to the Tukey honestly significant difference test ($p < 0.05$).

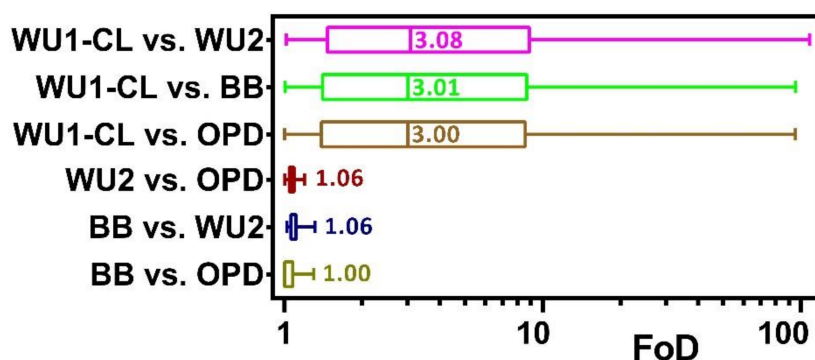


Figure 6. Box plots of the factor of difference, FoD, between the field-saturated hydraulic conductivity, K_{fs} ($\text{mm}\cdot\text{h}^{-1}$), data sets obtained by the BB, WU2, and OPD methods and the WU1 method with the cumulative linearization (CL) fitting method. The median values are also reported.

5. Discussion

Under the specific conditions encountered in this investigation, the transient analysis of single-ring data revealed that alternative procedures should be applied to properly analyze infiltration data, in order to avoid a misestimation of the soil hydraulic properties [66]. Specifically, the main reason for choosing other approaches was that invalid early data were detected in most cases with the CL method, and hence they were excluded from the analysis. The need to exclude the first data points when fitting the data was likely due to the highly sorptive nature of the sampled soils. Specifically, the porous media exhibited relatively low hydraulic conductivity compared to their sorptive capacity [37]. Indeed, cumulative infiltrations exhibited a marked concave part corresponding to the transient state and a linear part at the end of the curves related to the steady state [70]. This condition also made it difficult to estimate C_1 values due to the importance of the lateral capillary flow [65]. As a result, a reliable estimation of K_{fs} was unlikely. In other words, the generally poor performance of the fitting method spoiled the soil hydraulic characterization, affecting the general quality of the K_{fs} estimates and, thus, the comparison between the sampled sites and field campaigns. Indeed, this method relies on an infiltration model, i.e., Equation (8), that does not account for such a time evolution of soil properties between the early- and late-time infiltration stages responsible for the observed strong concavity of cumulative curves [71]. Moreover, it has to be remarked that the transient portion of the infiltration curves is frequently not usable to estimate steady-state infiltration rates, since it could be affected by several factors, including soil permeability, antecedent soil water content, ring radius and insertion depth (e.g., [1,13,21]). Although the poor performance of the CL method likely affected the reliability of the WU1 estimates, by increasing parameter variability, it has to be noted that the WU1 method allowed at least a check of the α^* value, which was selected a priori from the soil texture–structure categories to apply steady-state methods.

All steady-state methods revealed a slight but statistically significant K_{fs} decrease five years after the fire. These methods, with a characterization based exclusively on a stabilized infiltration process, yielded an appreciably lower variability of K_{fs} data compared to the WU1 method (Table 1). Steady-state methods were expected to give less variable K_{fs} estimates when compared to WU1, also as a consequence of the use of a fixed α^* value for the whole field, whereas variations of this parameter exist in the field depending on the texture and structure [1]. On the other hand, this assumption substantially facilitated the hydraulic characterization, yielding at the same time a sufficient level of accuracy for determining K_{fs} (e.g., [11,15,38]).

The considered soil properties unanimously highlighted the deterioration of the soil's physical quality after the fire. The results of this study suggested that the soil was not completely recovered five years after fire, and the negative effects resulting from the vegetation burning and soil organic matter removal have not yet been mitigated. One would expect that the degraded soil, i.e., with lower organic

matter and higher bulk density, could be more prone to runoff and erosion processes than the unburned soil [72]. However, despite common perceptions, Mediterranean vegetation adapts to fire and plant recolonization in burnt areas relatively quickly (e.g., [3,73,74]). According to many authors, vegetation recovering promptly reduces post-fire runoff and soil erosion rates (e.g., [75,76]). For instance, Cerdà and Doerr [9] observed, under Mediterranean environmental conditions, a fast recovery (2–4 years) of the terrain to pre-fire erosion rates. In our investigation, vegetation recovery, reaching 70% in 2017, could have had an effective role in preventing soil erosion. In other words, the prompt recovery of the vegetation cover may have mitigated the impacts of the worsening soil quality on erosion rates. In the future, erosion-focused studies may support the above hypothesis, increasing our understanding of the effects of soil impoverishment on erosion processes at the burnt sites.

6. Summary and Conclusions

In this study we analyzed changes in physical and hydrological soil properties few months and five years after a fire in a semi-arid environment in Eastern Spain. With this aim, we sampled both a burned and an unburned site and compared transient and steady-state analysis of single-ring infiltrometer data. The bottomless bucket method of Nimmo et al. [11] was selected in conjunction with other well-tested methods to estimate the field-saturated soil hydraulic conductivity. Any of the tested infiltration techniques appeared usable to obtain the order of magnitude of K_{fs} at the field sites. However, with the WU1 method, the variability in K_{fs} made it difficult to draw conclusions regarding the changes in the fire-affected soil. The choice of the method of soil hydraulic characterization led to contrasting conclusions, thus highlighting the need to choose the appropriate techniques. All the applied steady-state methods appeared more appropriate to detect and quantify slight changes in K_{fs} , whereas WU1 allowed at least a check of the selected α^* value. Our results showed a certain degree of soil degradation at the burnt site with an immediate reduction of the soil organic matter and a progressive increase of the soil bulk density during the five years following the fire. This general impoverishment resulted in a slight but significant decrease of the field-saturated soil hydraulic conductivity. A main implication of these results is the importance of long-term investigations of fire effects, since shorter-term studies may not always be sufficient for detecting and characterizing changes to the hydrological processes caused by a fire. This investigation also yielded encouraging signs on the applicability of the bottomless bucket method for a plausible estimation of K_{fs} . The comparison with other steady-state methods and the similarity of the results support this assessment.

Acknowledgments: The research leading to these results received funding from the POSTFIRE Project (CGL2013-47862-C2-1 and 2-R) and POSTFIRE_CARE Project (CGL2016-75178-C2-2-R). S.D.P. thanks M.J.K. for his contribution to keep the spirit up.

Author Contributions: All authors equally contributed to analyze the data, discuss the results, and write the manuscript.

Conflicts of Interest: The authors declare no conflict of interest.

References

1. Angulo-Jaramillo, R.; Bagarello, V.; Iovino, M.; Lassabatère, L. *Infiltration Measurements for Soil Hydraulic Characterization*; Springer International Publishing: New York, NY, USA, 2016; ISBN 978-3-319-31786-1.
2. Ebel, B.A.; Moody, J.A.; Martin, D.A. Hydrologic conditions controlling runoff generation immediately after wildfire. *Water Resour. Res.* **2012**, *48*, W03529. [[CrossRef](#)]
3. Certini, G. Effects of fire on properties of forest soils: A review. *Oecologia* **2005**, *143*, 1–10. [[CrossRef](#)] [[PubMed](#)]
4. Mataix-Solera, J.; Cerdà, A.; Arcenegui, V.; Jordán, A.; Zavala, L.M. Fire effects on soil aggregation: A review. *Earth-Sci. Rev.* **2011**, *109*, 44–60. [[CrossRef](#)]
5. Keesstra, S.; Wittenberg, L.; Maroulis, J.; Sambalino, F.; Malkinson, D.; Cerdà, A.; Pereira, P. The influence of fire history, plant species and post-fire management on soil water repellency in a Mediterranean catchment: The Mount Carmel range, Israel. *CATENA* **2017**, *149*, 857–866. [[CrossRef](#)]

6. Cerdà, A. Changes in overland flow and infiltration after a rangeland fire in a Mediterranean scrubland. *Hydrol. Process.* **1998**, *12*, 1031–1042. [[CrossRef](#)]
7. Novara, A.; Gristina, L.; Bodi, M.B.; Cerdà, A. The impact of fire on redistribution of soil organic matter on a mediterranean hillslope under maquia vegetation type. *Land Degrad. Dev.* **2011**, *22*, 530–536. [[CrossRef](#)]
8. Pereira, P.; Cerdà, A.; Úbeda, X.; Mataix-Solera, J.; Arcenegui, V.; Zavala, L.M. Modelling the Impacts of Wildfire on Ash Thickness in a Short-Term Period. *Land Degrad. Dev.* **2015**, *26*, 180–192. [[CrossRef](#)]
9. Cerdà, A.; Doerr, S.H. Influence of vegetation recovery on soil hydrology and erodibility following fire: An 11-year investigation. *Int. J. Wildland Fire* **2005**, *14*, 423–437. [[CrossRef](#)]
10. Lassabatere, L.; Angulo-Jaramillo, R.; Soria Ugalde, J.M.; Cuenca, R.; Braud, I.; Haverkamp, R. Beerkan estimation of soil transfer parameters through infiltration experiments—BEST. *Soil Sci. Soc. Am. J.* **2006**, *70*, 521. [[CrossRef](#)]
11. Nimmo, J.R.; Schmidt, K.M.; Perkins, K.S.; Stock, J.D. Rapid Measurement of Field-Saturated Hydraulic Conductivity for Areal Characterization. *Vadose Zone J.* **2009**, *8*, 142. [[CrossRef](#)]
12. Reynolds, W.D.; Elrick, D.E. Pondered Infiltration from a Single Ring: I. Analysis of Steady Flow. *Soil Sci. Soc. Am. J.* **1990**, *54*, 1233. [[CrossRef](#)]
13. Reynolds, W.D. Saturated hydraulic conductivity: Field measurement. In *Soil Sampling and Methods of Analysis*; Carter, M.R., Ed.; Canadian Society of Soil Science, Lewis Publishers: Boca Raton, FL, USA, 1993; pp. 599–613.
14. Ciollaro, G.; Lamaddalena, N. Effect of tillage on the hydraulic properties of a vertic soil. *J. Agric. Eng. Res.* **1998**, *71*, 147–155. [[CrossRef](#)]
15. Bagarello, V.; Iovino, M.; Elrick, D. A Simplified Falling-Head Technique for Rapid Determination of Field-Saturated Hydraulic Conductivity. *Soil Sci. Soc. Am. J.* **2004**, *68*, 66. [[CrossRef](#)]
16. Bagarello, V.; Baiamonte, G.; Castellini, M.; Di Prima, S.; Iovino, M. A comparison between the single ring pressure infiltrometer and simplified falling head techniques. *Hydrol. Process.* **2014**, *28*, 4843–4853. [[CrossRef](#)]
17. Gonzalez-Sosa, E.; Braud, I.; Dehotin, J.; Lassabatère, L.; Angulo-Jaramillo, R.; Lagouy, M.; Branger, F.; Jacqueminet, C.; Kermadi, S.; Michel, K. Impact of land use on the hydraulic properties of the topsoil in a small French catchment. *Hydrol. Process.* **2010**, *24*, 2382–2399. [[CrossRef](#)]
18. Fisher, D.K.; Gould, P.J. Open-Source Hardware Is a Low-Cost Alternative for Scientific Instrumentation and Research. *Mod. Instrum.* **2012**, *01*, 8–20. [[CrossRef](#)]
19. Di Prima, S. Automated single ring infiltrometer with a low-cost microcontroller circuit. *Comput. Electron. Agric.* **2015**, *118*, 390–395. [[CrossRef](#)]
20. Fisher, D.K.; Fletcher, R.S.; Anapalli, S.S.; Iii, H.C.P. Development of an Open-Source Cloud-Connected Sensor-Monitoring Platform. *Adv. Internet Things* **2017**, *8*, 1. [[CrossRef](#)]
21. Bagarello, V.; Di Prima, S.; Iovino, M.; Provenzano, G. Estimating field-saturated soil hydraulic conductivity by a simplified Beerkan infiltration experiment. *Hydrol. Process.* **2014**, *28*, 1095–1103. [[CrossRef](#)]
22. Alagna, V.; Bagarello, V.; Di Prima, S.; Iovino, M. Determining hydraulic properties of a loam soil by alternative infiltrometer techniques. *Hydrol. Process.* **2016**, *30*, 263–275. [[CrossRef](#)]
23. Bagarello, V.; Di Prima, S.; Iovino, M. Comparing Alternative Algorithms to Analyze the Beerkan Infiltration Experiment. *Soil Sci. Soc. Am. J.* **2014**, *78*, 724. [[CrossRef](#)]
24. Bagarello, V.; Di Prima, S.; Iovino, M. Estimating saturated soil hydraulic conductivity by the near steady-state phase of a Beerkan infiltration test. *Geoderma* **2017**, *303*, 70–77. [[CrossRef](#)]
25. Pachepsky, Y.A.; Guber, A.K.; Yakirevich, A.M.; McKee, L.; Cady, R.E.; Nicholson, T.J. Scaling and Pedotransfer in Numerical Simulations of Flow and Transport in Soils. *Vadose Zone J.* **2014**, *13*. [[CrossRef](#)]
26. Khodaverdiloo, H.; Khani Cheraghabdal, H.; Bagarello, V.; Iovino, M.; Asgarzadeh, H.; Ghorbani Dashtaki, S. Ring diameter effects on determination of field-saturated hydraulic conductivity of different loam soils. *Geoderma* **2017**, *303*, 60–69. [[CrossRef](#)]
27. Bagarello, V.; Santis, A.D.; Giordano, G.; Iovino, M. Source shape and data analysis procedure effects on hydraulic conductivity of a sandy-loam soil determined by ponding infiltration runs. *J. Agric. Eng.* **2017**, *48*, 71–80. [[CrossRef](#)]
28. Di Prima, S.; Bagarello, V.; Lassabatere, L.; Angulo-Jaramillo, R.; Bautista, I.; Burguet, M.; Cerdà, A.; Iovino, M.; Prosdocimi, M. Comparing Beerkan infiltration tests with rainfall simulation experiments for hydraulic characterization of a sandy-loam soil. *Hydrol. Process.* **2017**, *31*, 3520–3532. [[CrossRef](#)]

29. Di Prima, S.; Concialdi, P.; Lassabatère, L.; Angulo Jaramillo, R.; Pirastru, M.; Cerda, A.; Keesstra, S. Laboratory testing of Beerkan infiltration experiments for assessing the role of soil sealing on water infiltration. *CATENA* **2018**, submitted.
30. Haverkamp, R.; Bouraoui, F.; Zammit, C.; Angulo-Jaramillo, R. Soil properties and moisture movement in the unsaturated zone. In *The Handbook of Groundwater Engineering*, 3rd ed.; Taylor & Francis Group: Boca Raton, FL, USA, 1999.
31. Brooks, E.S.; Boll, J.; McDaniel, P.A. A hillslope-scale experiment to measure lateral saturated hydraulic conductivity. *Water Resour. Res.* **2004**, *40*, W04208. [[CrossRef](#)]
32. Castellini, M.; Di Prima, S.; Iovino, M. An assessment of the BEST procedure to estimate the soil water retention curve: A comparison with the evaporation method. *Geoderma* **2018**, *320*, 82–94. [[CrossRef](#)]
33. Di Prima, S.; Marrosu, R.; Lassabatere, L.; Angulo Jaramillo, R.; Pirastru, M. Determination of lateral preferential flow by combining plot- and point-scale infiltration experiments on a hillslope. *J. Hydrol.* **2018**, submitted.
34. Bagarello, V.; Castellini, M.; Di Prima, S.; Giordano, G.; Iovino, M. Testing a Simplified Approach to Determine Field Saturated Soil Hydraulic Conductivity. *Procedia Environ. Sci.* **2013**, *19*, 599–608. [[CrossRef](#)]
35. Touma, J.; Voltz, M.; Albergel, J. Determining soil saturated hydraulic conductivity and sorptivity from single ring infiltration tests. *Eur. J. Soil Sci.* **2007**, *58*, 229–238. [[CrossRef](#)]
36. Wu, L.; Pan, L. A generalized solution to infiltration from single-ring infiltrometers by scaling. *Soil Sci. Soc. Am. J.* **1997**, *61*, 1318–1322. [[CrossRef](#)]
37. Yilmaz, D.; Lassabatere, L.; Angulo-Jaramillo, R.; Deneele, D.; Legret, M. Hydrodynamic Characterization of Basic Oxygen Furnace Slag through an Adapted BEST Method. *Vadose Zone J.* **2010**, *9*, 107. [[CrossRef](#)]
38. Wu, L.; Pan, L.; Mitchell, J.; Sanden, B. Measuring Saturated Hydraulic Conductivity using a Generalized Solution for Single-Ring Infiltrimeters. *Soil Sci. Soc. Am. J.* **1999**, *63*, 788. [[CrossRef](#)]
39. White, I.; Sully, M.J. Macroscopic and microscopic capillary length and time scales from field infiltration. *Water Resour. Res.* **1987**, *23*, 1514–1522. [[CrossRef](#)]
40. Philip, J. The theory of infiltration: 4. Sorptivity and algebraic infiltration equations. *Soil Sci.* **1957**, *84*, 257–264. [[CrossRef](#)]
41. Smiles, D.; Knight, J. A note on the use of the Philip infiltration equation. *Soil Res.* **1976**, *14*, 103–108. [[CrossRef](#)]
42. Soil Survey Staff. *Keys to Soil Taxonomy*, 12th ed.; USDA-Natural Resources Conservation Service: Washington, DC, USA, 2014.
43. Di Prima, S.; Rodrigo-Comino, J.; Novara, A.; Iovino, M.; Pirastru, M.; Keesstra, S.; Cerda, A. Assessing soil physical quality of citrus orchards under tillage, herbicide and organic managements. *Pedosphere*. in press.
44. Mubarak, I.; Mailhol, J.C.; Angulo-Jaramillo, R.; Ruelle, P.; Boivin, P.; Khaledian, M. Temporal variability in soil hydraulic properties under drip irrigation. *Geoderma* **2009**, *150*, 158–165. [[CrossRef](#)]
45. Xu, X.; Kiely, G.; Lewis, C. Estimation and analysis of soil hydraulic properties through infiltration experiments: Comparison of BEST and DL fitting methods. *Soil Use Manag.* **2009**, *25*, 354–361. [[CrossRef](#)]
46. Bagarello, V.; Di Prima, S.; Iovino, M.; Provenzano, G.; Sgroi, A. Testing different approaches to characterize Burundian soils by the BEST procedure. *Geoderma* **2011**, *162*, 141–150. [[CrossRef](#)]
47. Alagna, V.; Bagarello, V.; Di Prima, S.; Giordano, G.; Iovino, M. Testing infiltration run effects on the estimated water transmission properties of a sandy-loam soil. *Geoderma* **2016**, *267*, 24–33. [[CrossRef](#)]
48. Alagna, V.; Di Prima, S.; Rodrigo-Comino, J.; Iovino, M.; Pirastru, M.; Keesstra, S.D.; Novara, A.; Cerdà, A. The Impact of the Age of Vines on Soil Hydraulic Conductivity in Vineyards in Eastern Spain. *Water* **2017**, *10*, 14. [[CrossRef](#)]
49. Walkley, A.; Black, I.A. An examination of the Degtjareff method for determining soil organic matter, and a proposed modification of the chromic acid titration method. *Soil Sci.* **1934**, *37*, 29–38. [[CrossRef](#)]
50. Mataix-Solera, J.; Doerr, S. Hydrophobicity and aggregate stability in calcareous topsoils from fire-affected pine forests in southeastern Spain. *Geoderma* **2004**, *118*, 77–88. [[CrossRef](#)]
51. Cerdà, A.; Doerr, S.H. Soil wettability, runoff and erodibility of major dry-Mediterranean land use types on calcareous soils. *Hydrol. Process.* **2007**, *21*, 2325–2336. [[CrossRef](#)]
52. Wang, Z.; Wu, L.; Wu, Q.J. Water-entry value as an alternative indicator of soil water-repellency and wettability. *J. Hydrol.* **2000**, *231–232*, 76–83. [[CrossRef](#)]

53. Alagna, V.; Iovino, M.; Bagarello, V.; Mataix-Solera, J.; Lichner, L. Application of minidisk infiltrometer to estimate water repellency in Mediterranean pine forest soils. *J. Hydrol. Hydromech.* **2017**, *65*. [[CrossRef](#)]
54. Di Prima, S.; Bagarello, V.; Angulo-Jaramillo, R.; Bautista, I.; Cerdà, A.; del Campo, A.; González-Sanchis, M.; Iovino, M.; Lassabatere, L.; Maetzke, F. Impacts of thinning of a Mediterranean oak forest on soil properties influencing water infiltration. *J. Hydrol. Hydromech.* **2017**, *65*, 276–286. [[CrossRef](#)]
55. Bagarello, V.; Iovino, M.; Reynolds, W. Measuring hydraulic conductivity in a cracking clay soil using the Guelph permeameter. *Trans. ASAE* **1999**, *42*, 957–964. [[CrossRef](#)]
56. Elrick, D.E.; Reynolds, W.D. Methods for analyzing constant-head well permeameter data. *Soil Sci. Soc. Am. J.* **1992**, *56*, 320. [[CrossRef](#)]
57. Mohanty, B.P.; Kanwar, R.S.; Everts, C.J. Comparison of saturated hydraulic conductivity measurement methods for a glacial-till soil. *Soil Sci. Soc. Am. J.* **1994**, *58*, 672–677. [[CrossRef](#)]
58. Warrick, A.W. Spatial variability. In *Environmental Soil Physics*; Hillel, D., Ed.; Academic Press: San Diego, CA, USA, 1998; pp. 655–675.
59. Lee, D.M.; Elrick, D.E.; Reynolds, W.D.; Clothier, B.E. A comparison of three field methods for measuring saturated hydraulic conductivity. *Can. J. Soil Sci.* **1985**, *65*, 563–573. [[CrossRef](#)]
60. Reynolds, W.D.; Drury, C.F.; Tan, C.S.; Fox, C.A.; Yang, X.M. Use of indicators and pore volume-function characteristics to quantify soil physical quality. *Geoderma* **2009**, *152*, 252–263. [[CrossRef](#)]
61. García-Oliva, F.; Sanford, R.L.; Kelly, E. Effects of slash-and-burn management on soil aggregate organic C and N in a tropical deciduous forest. *Geoderma* **1999**, *88*, 1–12. [[CrossRef](#)]
62. Kane, E.S.; Kasischke, E.S.; Valentine, D.W.; Turetsky, M.R.; McGuire, A.D. Topographic influences on wildfire consumption of soil organic carbon in interior Alaska: Implications for black carbon accumulation. *J. Geophys. Res. Biogeosci.* **2007**, *112*, G03017. [[CrossRef](#)]
63. Ebel, B.A.; Moody, J.A. Rethinking infiltration in wildfire-affected soils. *Hydrol. Process.* **2013**, *27*, 1510–1514. [[CrossRef](#)]
64. Rawls, W.J.; Pachepsky, Y.A.; Ritchie, J.C.; Sobecki, T.M.; Bloodworth, H. Effect of soil organic carbon on soil water retention. *Geoderma* **2003**, *116*, 61–76. [[CrossRef](#)]
65. Vandervaere, J.-P.; Vauclin, M.; Elrick, D.E. Transient flow from tension infiltrometers I. The two-parameter equation. *Soil Sci. Soc. Am. J.* **2000**, *64*, 1263–1272. [[CrossRef](#)]
66. Vandervaere, J.-P.; Vauclin, M.; Elrick, D.E. Transient Flow from Tension Infiltrometers II. Four Methods to Determine Sorptivity and Conductivity. *Soil Sci. Soc. Am. J.* **2000**, *64*, 1272–1284. [[CrossRef](#)]
67. Lassabatere, L.; Angulo-Jaramillo, R.; Soria-Ugalde, J.M.; Šimůnek, J.; Haverkamp, R. Numerical evaluation of a set of analytical infiltration equations: EVALUATION INFILTRATION. *Water Resour. Res.* **2009**, *45*. [[CrossRef](#)]
68. Carsel, R.F.; Parrish, R.S. Developing joint probability distributions of soil water retention characteristics. *Water Resour. Res.* **1988**, *24*, 755–769. [[CrossRef](#)]
69. White, I.; Sully, M.J. On the variability and use of the hydraulic conductivity alpha parameter in stochastic treatments of unsaturated flow. *Water Resour. Res.* **1992**, *28*, 209–213. [[CrossRef](#)]
70. Di Prima, S.; Lassabatere, L.; Bagarello, V.; Iovino, M.; Angulo-Jaramillo, R. Testing a new automated single ring infiltrometer for Beerkan infiltration experiments. *Geoderma* **2016**, *262*, 20–34. [[CrossRef](#)]
71. Poulouvassilis, A.; Elmaloglou, S.; Kerkides, P.; Argyrokastritis, I. A variable sorptivity infiltration equation. *Water Resour. Manag.* **1989**, *3*, 287–298. [[CrossRef](#)]
72. Cerdà, A. The influence of aspect and vegetation on seasonal changes in erosion under rainfall simulation on a clay soil in Spain. *Can. J. Soil Sci.* **1998**, *78*, 321–330. [[CrossRef](#)]
73. Badalamenti, E.; Gristina, L.; Laudicina, V.A.; Novara, A.; Pasta, S.; Mantia, T.L. The impact of *Carpobrotus* cfr. *acinaciformis* (L.) L. Bolus on soil nutrients, microbial communities structure and native plant communities in Mediterranean ecosystems. *Plant Soil* **2016**, *409*, 19–34. [[CrossRef](#)]

74. Pasta, S.; Badalamenti, E.; Mantia, T.L. *Acacia cyclops* A. Cunn. ex G. Don (Leguminosae) in Italy: First cases of naturalization. *An. Jardín Botánico Madr.* **2012**, *69*, 193–200. [[CrossRef](#)]
75. Moody, J.A.; Martin, D.A. Initial hydrologic and geomorphic response following a wildfire in the Colorado Front Range. *Earth Surf. Process. Landf.* **2001**, *26*, 1049–1070. [[CrossRef](#)]
76. Castellini, M.; Iovino, M.; Pirastru, M.; Niedda, M.; Bagarello, V. Use of BEST Procedure to Assess Soil Physical Quality in the Baratz Lake Catchment (Sardinia, Italy). *Soil Sci. Soc. Am. J.* **2016**. [[CrossRef](#)]



© 2018 by the authors. Licensee MDPI, Basel, Switzerland. This article is an open access article distributed under the terms and conditions of the Creative Commons Attribution (CC BY) license (<http://creativecommons.org/licenses/by/4.0/>).